Title

Multi-omic Analyses of Extensively Decayed Pinus contorta Reveal Expression of a Diverse Array of Lignocellulose-Degrading Enzymes

Journal

Applied and Environmental Microbiology, 84(20)

ISSN

0099-2240

Authors

Hori, Chiaki
Gaskell, Jill
Cullen, Dan
et al.

Publication Date

2018-10-15

DOI

10.1128/aem.01133-18

Peer reviewed

Multi-omic analyses of extensively decayed *Pinus contorta* reveal expression of diverse array of lignocellulose degrading enzymes

Chiaki Hori,[a] Jill Gaskell,[b] Dan Cullen,[b] Grzegorz Sabat,[c] Philip E. Stewart,[d] Kathleen Lail,[e] Yi Peng,[e] Kerrie Barry,[e] Igor V. Grigoriev,[e,f] Annegret Kohler[g], Laure Fauchery[g], Francis Martin,[g] Carolyn A. Zeiner,[h] Jennifer M. Bhatnagar[h]

[a]School of Engineering, Hokkaido University, Sapporo, Japan

[b]USDA, Forest Products laboratory, Madison, Wisconsin, USA

[c]University of Wisconsin-Madison Biotechnology Center, Madison, Wisconsin, USA

[d]Rocky Mountain Laboratories, NIAID, NIH, Hamilton, Montana, USA

[e]US Department of Energy Joint Genome Institute, Walnut Creek, California, USA

[f]Department of Plant and Microbial Biology, University of California Berkeley, Berkeley, California, USA

[g]Institut National de la Recherche Agronomique, Unité Mixte de Recherche 1136, Institut National de la Recherche Agronomique-Université de Lorraine, Interactions Arbres/Micro-organismes, 54280 Champenoux, France

[h]Department of Biology, Boston University, Boston, Massachusetts, USA

ABSTRACT Fungi play a key role cycling nutrients in forest ecosystems but the mechanisms remain uncertain. To clarify the enzymatic processes involved in wood decomposition, metatranscriptomics and metaproteomics of extensively decayed lodgepole pine were examined by RNAseq and LC-

MS/MS, respectively. Following *de novo* metatranscriptome assembly, 52,011 contigs were searched for functional domains and homology to database entries. Contigs similar to to basidiomycete transcripts dominated and many of these were most closely related to ligninolytic white rot fungi or cellulolytic brown rot fungi. A diverse array of carbohydrate active enzymes (CAzymes) representing a total of 132 families or subfamilies were identified. Among these were 672 glycoside hydrolases including highly expressed cellulases or hemicellulases. The CAzymes also included 162 genes encoding redox enzymes classified within Auxiliary Activity (AA) families. Eighteen of these were manganese peroxidases, key components of ligninolytic white rot fungi. Expression of other redox enzymes supported the working of hydroquinone reduction cycles capable of generating reactive hydroxyl radical. The latter has been implicated as a diffusible oxidant responsible for cellulose depolymerization by brown rot fungi. Thus, enzyme diversity and the coexistence of brown and white rot fungi suggest complex interactions of fungal species and degradative strategies during the decay of logdepole pine.

IMPORTANCE The deconstruction of recalcitrant woody substrates is a central component of carbon cycling and forest health. Laboratory investigations have contributed substantially toward understanding mechanisms employed by model wood decay fungi, but few studies have examined the physiological processes in natural environments. Herein, we identify the functional genes present in field samples of extensively decayed lodgepole pine (*Pinus contorta*), a major species distributed throughout the North American Rocky Mountains. The classified transcripts and proteins revealed a diverse array of oxidative and hydrolytic enzymes involved in the degradation of lignocellulose. The evidence also strongly supports simultaneous attack by fungal species employing different enzymatic strategies.

Fungi play a critical role in recycling of forest carbon via wood decomposition. Significant effort has focused on describing the microbial communities using conventional plating techniques, observations of conspicuous fungal fruiting bodies (1), enzyme assays (2) and metagenomics analyses of rRNA and other conserved genes (3-5). The complexity and interactions among physiologically active wood decay microbes remain poorly understood, although recent work on forest soils and litter may be relevant, at least in terms of experimental tools (6-11).

Two forms of wood decay are generally recognized (12, 13). Brown rot fungi rapidly depolymerize cellulose via oxidative systems. Bulk lignin is left behind as a polymeric residue. In contrast, white rot fungi degrade and metabolize lignin while cellulose is hydrolyzed by conventional Carbohydrate Active Enzymes (CAzymes) (14). Except for rare cases (15), genome annotation supports these classifications; white rot fungi feature genes encoding ligninolytic peroxidases and numerous cellulases while brown rot fungi have few, if any, of these genes (16). Efficient degradation and mineralization of native lignin are accomplished almost exclusively by white rot basidiomycetes, some of which are closely related to brown rot fungi. The efficiency by which these fungi degrade cellulose and lignin has generated considerable interest in bioprocess development.

Toward the identification of enzymes directly involved in the natural decomposition of wood, metatranscriptome and metaproteome investigations were performed on decayed lodgepole pine (*Pinus contorta*), a fire-adapted species widely distributed throughout the North American Rocky Mountains.

RESULTS

Metatranscriptome. Analyses were focused on Poly(A) RNA purified from extensively decayed lodgepole pine samples collected in western Montana national forests. To provide a broad perspective, sampling included distinct locations and fire histories. Avoiding direct contact with soil/litter, the loose material was collected from the logs' upper surface. A total of 2.9 X 10^8 Illumina-RNA-Seq reads were generated from the amplified poly(A) RNA. De novo assembly yielded 274,233 contigs, each with a minimum of 100 reads. To add confidence to BLASTx queries, these were further filtered to 52,011 contigs over 750 bp in length (Table 1).

BLASTx searches of metatranscriptome contigs against NCBI RefSeq, GO, InterPro and EC supported putative classifications and revealed conserved protein domains directly supporting function and/or features potentially involved (e.g. secretion signals, transmembrane helices) (Table 1). Using a conservative e-value threshold (10^{-15}), 41% of the contigs were related only to hypothetical proteins or otherwise unassigned (Figure 1). A total of 1,316 putative CAzyme-encoding transcripts were identified. Impressive numbers of transporters (1,631) and cytochrome P450s (203) were also found and, although their precise function is difficult to predict, some are likely to play an important role in the uptake and metabolism of low molecular weight products during cell wall degradation. A substantial number of extracellular proteases together with oligopeptide and amino acid transporters (Dataset S1) are probably indicative of nitrogen scavenging within the N-limited substrate. Not surprisingly, approximately 50% of the Refseq hits were encoding intracellular structural proteins (e.g. actin) or enzymes involved in protein synthesis (e.g. ribosomal proteins) and central metabolism (e.g. Glyceraldehyde-3-phosphate dehydrogenase). Without doubt, relaxing blast thresholds and/or

92 inclusion of contigs < 750 bp would identify additional sequences, possibly including those encoding
93 small secreted proteins (17). A detailed description of contigs is presented in supplemental Dataset S1.
94 Of the 1,316 CAzymes, 162 were classified as members of an Auxiliary Activities (AA) family
95 (Figure 2; (18). Clearly demonstrating white rot ligninolysis, eight contigs encoding manganese-
96 dependent lignin peroxidases (MnPs) were among the 30 most highly expressed AA-encoding genes
97 (Table 2). Abundant transcripts corresponding to eight alcohol oxidases were also identified, and all
98 were closely related to *Gloeophyllum trabeum* methanol oxidase (19). Two benzoquinone reductases
99 may participate in a redox cycle tied to hydroxyl radical generation during brown rot decay (20-22).
100 Surprisingly, the highest transcript levels among AA-encoding genes were attributed to lytic
101 polysaccharide monooxygenases (LPMO; Table 2). Previously classified as GH61s, these copper
102 dependent enzymes have been shown to cleave C1 or C4 glycosidic bonds [reviewed in Ref. (23)].
103 Beyond the AA families, 1,154 additional CAzymes were identified, including 672 glycoside
104 hydrolases (GHs), 154 glycosyl transferases (GTs), 105 carbohydrate esterases (CEs), 13
105 polysaccharide lyases (PLs) and 210 carbohydrate binding modules. Glycoside hydrolase families
106 associated with cellulose degradation, e.g. GH5_5, GH6, GH7, GH12, GH45, were particularly
107 abundant (Figure 3; Table 3). Total transcripts classified as the 'exo'-acting cellobiohydrolases (GH7s
108 and GH6s) were substantially increased due to the activity of relatively few, but highly expressed
109 genes (Figure 3). Similarly, of 25 GH5_5 contigs, 4921502_1 and 1142146_1 (Table 3)
110 disproportionately contributed 45% of the total reads (Figure 3; Dataset S1). Families GH7, GH6 and
111 GH5_5 accounted for 25%, 15% and 15% of the cellulase reads, respectively.
112 Enzymes broadly characterized as hemicellulases were among the most highly expressed
113 transcripts and included GH114 Endo α-1-4-polygalactosaminidase (3859657_1), GH10 endo- 1,4-β
114 xylanase (3561636_2), GH53 endo-1,4-β-galactanase and a GH27 α-galactosidase (910111_1) (Table

115 3). The numbers of contigs and total reads assigned to potential hemicellulase families are shown on
116 Figure 4. Several of these are involved in the degradation of galactoglucomannan,
117 arabinoglucuronoxylan and arabinogalactan, all of which are components of softwood hemicellulose.
118 The complete breakdown of these substrates may involve the combined activities of multiple GH
119 families. For example, β-mannanases belonging to GH2, GH5_7 and GH5-41 represented 15% of the
120 hemicellulose-assigned reads (Dataset S1). In addition to plant cell wall degradation, β-1,3-glucans and
121 chitin from insects and fungal cell walls are likely substrates for GHs such as GH18 chitinases. Beyond
122 these hydrolases, CEs associated with the removal of acetyl substitution from hemicellulose and chitin
123 (CE1, CE4 and CE16) were major components of the transcriptome (Dataset S1).
124 Contigs with putative functions were most frequently related to basidiomycetes (Figure 5, 3S;
125 Dataset S1), although sequences closely related to other eukaryotes, or their viruses, were also
126 detected. Of the 52,011 contigs, 39,765 gave significant BLASTx scores e-values ($<10^{15}$) to the NCBI
127 Refseq database. Translations of these contigs, plus the extended ORFs of those contigs without
128 significant BLASTx scores, were queried against the NCBI non-redundant (NR) protein database. A
129 total of 39,973 proteins gave significant hits (e-values $<10^{15}$), and these were distributed among 2,810
130 species including 1,387 species with a single hit. Forty-two species accounted for approximately 50%
131 of the top BLASTp hits (Figure 5, Panel A). This overall pattern of similarity to basidiomycete genes
132 was also observed for a much smaller subset of 1,316 CAZy-encoding genes (Figure 5 panel B). The
133 skewed representation toward basidiomycetes is also evident when considering up to ten database
134 entries most closely related to each contig (Fig. 3S).
135 Many genes involved in lignocellulose deconstruction were highly expressed including the
136 abovementioned exo- and endo-acting cellulases, transporters and oxidoreductases (Tables 2, 3 and
137 S1). In some instances, possible prokaryote sequences were detected. For example, the predicted

amino acid sequence of 1384861_1, a putative cellobiohydrolase (Table 3), was 43% (e-value 10^{-102}) identical to *Sorangium cellulosum* (KYG02679). However, the contig sequence is also similar to various fungal accessions such as OAL51409 from *Pyrenochaeta sp.*but polyadenylation is absent, as expected if originating from prokaryotic organisms. Evidence supporting the prokaryotic origins of other highly expressed genes is more compelling. Specifically, contigs 94066_1, 4739131_4 and 2374420_1 are among the 30 most highly expressed glycoside hydrolases (Table 3) and most closely related to *Kutzneria sp* WP_084578858), *Enhygromyxa salina* (KIG15205) and *Actinobacteria bacteria* (OLB81315) genes, respectively (Dataset S1). All have short 3' poly(A) tracts of 16 to 24 residues and, in each case, the 10 most closely related database entries are also derived from bacterial.

A total of 28 contigs were most closely related to cDNAs derived from an "uncultured eukaryote" in *Picea abies* forest soils (7). Twenty-two of these encode putative CAZy domains (Dataset S1). The deduced amino acid sequence of a highly expressed GH45-encoding gene (4034495_1; Table 3) is 76% identical to accession CCA94939 (7).

Metaproteome. MS/MS data matched 1,964 proteins corresponding to 1,935 contigs. Of these mass spectrometry-identified proteins, the majority were encoded by orthologous sets of housekeeping genes such as 40S and 60S ribosomal proteins, actin and glyceraldehyde-3-phosphate dehydrogenase (Dataset S1). Sixty-seven proteins corresponded to hypothetical proteins, 42 were predicted proteins and 62 were not assigned by NR BLASTp. On the other hand, 24 proteins were classified by Auxiliary Activities, and four Dye Decolorizing Peroxidases (DyP; Reviewed in Ref. (24)) were also identified (Table 4). Other CAzymes included 11 carbohydrate esterases and 23 glycoside hydrolases categorized as cellulases and hemicellulases (Table 5). The semi-quantitative measures of protein abundance were not correlated with the number of reads, a common observation often related to solubility and cellular targeting (intracellular, extracellular, membrane bound), protein stability, substrate binding, molecular

161 weight and/or access to trypsin cleavage sites. Previous studies have shown high numbers of
162 basidiomycetous proteins in forest litter, an observation attributed to relatively high C/N ratios (11,
163 25).

164 Enzymatic activities of cellobiohydrolase, β-1,4 glucosidase, α-1,4-glucosidase, β-1,4-N-
165 acetylglucosaminidase, β-1,4-xylosidase, β-glucuronidase, L-leucine aminopeptidase and peroxidase
166 activity were detected at the three sampling points (Fig. S3). Because no laccase transcripts or proteins
167 could be clearly identified, polyphenol oxidase activity may be due to non-specific oxidations of the L-
168 DOPA substrate (Table S4). However, other multicopper oxidases, including ferroxidase-like enzymes
169 (5217211_1, 2197006_3, 1400590_1; Dataset S1), may have contributed to the L-DOPA activity.

170

171

172 **DISCUSSION**

173 Filamentous fungi play a key role in depolymerizing, degrading and mineralizing the major
174 components of woody cell walls, including cellulose, hemicellulose and the recalcitrant lignin. Only a
175 fraction of the species has been isolated in pure culture. Moreover, the laboratory conditions employed
176 with model white rot and brown rot fungi fail to mimic natural decay processes. To identify key
177 enzymes and further understand lignocellulose deconstruction we have examined the
178 metatranscriptome and metaproteome of extensively decayed lodgepole pine. In aggregate, the results
179 support complex enzymatic interactions carried out by diverse microbial communities.

180 The majority of the classified sequences were most closely related to Basidiomycota, followed by
181 cellulolytic Ascomycota, slime molds and other Protista. Species-level taxonomic assignments are
182 likely biased by the skewed representation of genomes available in the NCBI databases. This is
183 particularly problematic when discriminating brown rot and white rot fungi (15), unless certain white

184 rot-specific genes are detected such as the MnPs (Table 2, S1). In aggregate, our results strongly
185 suggest that both white and brown rot fungi are simultaneously active in decaying lodgepole pine
186 (Fig.5 and 3S). Our analysis cannot resolve fine spatial relationships between fungi and their
187 interactions (e.g. mutualistic, antagonistic, neutral) remain uncertain. However, the findings are
188 consistent with the coexistence of white and brown rot fungi following laboratory inoculation of spruce
189 logs and placement in forest settings (5, 26, 27). More recently, ITS2 analyses of Norway spruce
190 (*Picea abies*) logs in unmanaged stands identified various basidiomycetes, including several white and
191 brown rot species (28). Mäkipää et al reported that most species were rare and that the top 30
192 accounted for 50% of all OTUs (28). Our BLASTp counts suggest similar levels of species richness,
193 with the top 30 hits accounting for 43% (18,952) of the contigs. However, we did not observe abundant
194 mycorrhizal species (28), and our results surely underestimate species diversity because of the
195 dependency on physiological activity as well as the lability of RNA targets. These results stand in
196 contrast to metatransciptome investigations of *Pinus taeda* where few mycorrhizal species are active
197 (29). In this context, we recognize that the observed patterns would be quite different on other wood
198 species during wet and/or cool conditions. Our sampling was confined to *P. contorta*, during a dry
199 period in early summer and, although sampling was not designed to invite statistically valid
200 comparisons, there seemed relatively little difference in the fire-disturbed versus undisturbed samples
201 (Table S2; Fig. S1 and S2).

202 Unexpectedly, the second most common top BLAST hits were *Phialocephala spp.* (Fig. 5 and 2S).
203 A well-established endophyte of conifer needles, *P. scopiformis* produces the anti-insectan compound
204 rugulosin and confers increased tolerance to spruce budworm. The root endophyte *Phialocephala*
205 *subalpina* (30, 31) is closely related to *P. scopiformis* and, together, these species constitute 5.8%
206 (2,542) of the total number of top hits. Possibly, an undescribed *Phialocephala* sp or variant strain

encode the observed transcripts and peptides. The genomes of *P. scopiformis* (32) and *P. subalpina* feature numerous CAzymes and, in view of the expression patterns reported here, it seems probable that filamentous basidiomycetes and ascomycetous *Phialocephala spp.* participate in the late stages of *P. contorta* decay.

Our analyses identified an array of genes directly and indirectly involved in lignocellulose degradation. Eighteen MnP-encoding contigs were present (Dataset S1), and peptides matching eight of these were detected (Dataset S1). Generally considered ligninolytic enzymes, amino acid alignments were 53% to 67% identical to *Phanerochaete chrysosporium* MnP1 (accession Q02567) and, within aligned regions, key residues involved in Mn binding and catalysis were conserved (33). In contrast to MnPs, which are widely distributed among white rot fungi (12, 34), lignin peroxidases and versatile peroxidases were not detected. We also observed an array of alcohol oxidases (AA3_3s) that may play a role in supplying extracellular H_2O_2 to the peroxidases. The role of six DyP peroxidases, three heme-thiolate peroxidases (HTPs) and six chloroperoxidases in ligninolysis, if any, remains unclear (35). Transcripts and activities of these enzymes have been reported in forest litter (36) and, although lacking the oxidative potential to attack lignin, they may be involved in the oxidation and hydroxylation of aromatic metabolites derived from lignin (35). The peptides corresponding to four Dyp genes were identified, but none detected for the chloroperoxidases and HTPs. Neither transcripts or peptides were identified for laccases suggesting no significant role in ligninolysis, at least in the late stages of wood decay.

Other redox enzymes assigned to AA families provide additional insight into degradative mechanisms. We were unable to detect LPMO peptides by MS/MS, but the genes (AA9) were particularly numerous and the transcripts abundant with 65 contigs and 93,889 transcripts (Table 2; Figure 2; Dataset S1). Assuming these Cu-dependent enzymes are secreted, they likely play an

important role in cellulose cleavage, especially the 12 genes that feature a CBM1 domain (Dataset S1). They may also oxidize xyloglucan and glucomannans as recently demonstrated for a LPMO from the brown rot fungus *Gloeophyllum trabeum* (37). Interestingly, LPMO activity was recently shown dependent on H_2O_2 (38). This may partly explain the number (26), high transcript levels (60,929 reads) and Peptide Spectrum Matches (PSMs) of putative alcohol oxidases (Table 2, 5 and S1). These family AA3 enzymes generate peroxide from various substrates, including methanol. Both white rot and brown rot fungi demethylate lignin and, in the case of *Gloeophyllum trabeum* brown rot, evidence suggests that methanol oxidase contributes peroxide to advance the Fenton reaction (19).

The mechanism(s) of brown rot decay remain unsettled. Recent genome annotations make clear that cellobiose dehydrogenase is not essential, as this multifunctional enzyme is absent from the genome of several efficient brown rot fungi. Our analysis also failed to identify the transcript in decayed lodgepole pine. On the other hand, the data is consistent with hydroxyl radicals generated via benzoquinone reductase and oxalate-Fe^{3+} chelates (20-22). Specifically, we identified 25 putative benzoquinone reductases (32,831 reads), 20 oxalate decarboxylases (28,450 reads) and an oxalate transporter which, together, may modulate hydroxyl radical production (39)(Dataset S1). In contrast, our inability to detect any laccase transcripts undermines its involvement in the process (40-42).

Without doubt, lodgepole pine decay involves the combined activities of functionally diverse enzymes and fungal species. The synergistic activities of conventional endo- and exocellobiohydrolases are well known. More recently, LPMO has been shown to boost the performance of these hydrolases (43, 44). Although our study selected for eukaryotic mRNA, genes most closely related to bacteria were occasionally identified. Several studies have implicated bacteria as part of complex consortia involved in wood decay (45-48); reviewed in Ref. (49). We also found genes most closely related to slime molds and other protists as well as several bacteria many of which

253 have been associated with decomposition. The enzymatic machinery and interactions among these
254 species merit further investigation.
255
256 **MATERIALS AND METHODS**
257 **Sample description and RNA preparation.** Loose and crumbling material from the upper
258 surface of three extensively decayed lodgepole pine logs were collected in western Montana July,
259 2014. The logs were in direct contact with the ground. No clear zones of fungal colonization or fruiting
260 bodies were observed on the decayed wood or in the immediate vicinity. However, portions of the
261 decayed surfaces had dark cubicle regions interspersed with lighter colored fibrous areas, often
262 associated with brown rot and white rot, respectively (Figure S5). Locations included U.S. Forest
263 Service's Tenderfoot Creek Experimental Forest (TCEF) at 46.923333, -110.869444 (N 46 55' 24" W
264 110 52" 10) (Altitude 2238 m). This specific site was within a mature lodgepole pine stand with a
265 dense canopy, sparse ground cover and no history of fire in over 140 years. Two samples were
266 collected near Gibbon's Pass, on the Bitterroot National Forest, MT. The area was the site of a
267 catastrophic fire in 2001 and, at the time of collection, featured a dense stand of lodgepole saplings.
268 Considerable ground cover was predominantly *Xerophyllum tenax, Lupinus sericeus* and *Vaccinium*
269 *scoparium*. The GP1 log was in a relatively flat area at 45.754444, -113.909444 (N 45 45' 16" W
270 113.54' 34) (altitude 2146 m), whereas the GP2 log was located on an incline at 45.755278, -
271 113.910556 (N 45 45' 19" W 113.54' 38) (altitude 2138 m). The length of time during which the trees
272 were down could not be determined, although at the time of fall, cellulose, hemicellulose and lignin are
273 estimated to be 44%, 31%, and 27%, respectively (50). All samples were ground with an electric blade
274 coffee grinder, passed through a 2 mm sieve, shipped overnight on ice and stored at -80C.

Approximately 1 gram of the ground samples were extracted with the MO BIO RNA Isolation Kit (Carlsbad, CA; catalog # 12866-25) according to the manufacturer's recommendations. The final total RNA pellet was suspended in 100 ul water. Oligo $(dT)_{25}$ Dynabeads (Oslo, Norway) was prepared as suggested by the manufacturer. Seventy microliters of the beads were washed and suspended in 100 µL of binding buffer (20mM Tris-HCl, pH 7.5, 1.0M LiCl, 2mM EDTA). To eliminate secondary structure, RNA was incubated at 65˚C for 2 minutes and immediately placed on ice. The RNA and bead solution were mixed and, after occasional inverting over a 5 min period, placed in a Dynal magnet stand. The beads were washed and re-captured twice and the Poly(A) RNA eluted with 10 ul water. The Poly(A) RNA was incubated at 70˚C for 10 minutes and amplified following the MessageAmp II protocol (Invitrogen, ThermoFisher Scientific). The aRNA quantity and quality were assessed by a Qubit fluorometer (ThermoFisher Scientific) and a 2100 BioAnalyzer (Agilent), respectively.

RNA-Seq libraries were prepared and sequenced by the U.S. Department of Energy Joint Genome Institute (Walnut Creek, CA). mRNA was fragmented and reversed transcribed using random hexamers and SSII (Invitrogen) followed by second strand synthesis. The fragmented cDNA was treated with end-pair, A-tailing, adapter ligation, and eight cycles of PCR. qPCR was used to determine the concentration of the libraries. The prepared libraries were quantified using KAPA Biosystem's next-generation sequencing library qPCR kit and run on a Roche LightCycler 480 real-time PCR instrument. The quantified libraries were then prepared for sequencing on the Illumina HiSeq sequencing platform utilizing a TruSeq paired-end cluster kit, v4, and Illumina's cBot instrument to generate a clustered flowcell for sequencing. Sequencing of the flowcell was performed on the Illumina HiSeq-1TB sequencer using HiSeq TruSeq SBS sequencing kits, v4, following a 2x150 indexed run recipe. Fastq files were deposited in the Sequence Reads Archive under biosample

accessions SAMN07573382 (GP1), SAMN07573383 (TCEF) and SAMN07573384 (GP2). The three sample files were combined, without normalization, for final assembly. DNASTAR's SeqMan NGen (v 14.1) was used to perform *de novo* transcriptome assemblies with default parameters (mer size:21; clustering match: 97%) with a minimum of 101 sequences per contig (average: 590). The resulting assemblies were sorted according to the number of reads and length with SeqMan Pro. Those contigs exceeding 750 bp were initially BLASTx queried against the Refseq protein database and EMBL-EBI was used to predict Interpro domains as well as transmembrane helices, secretion signals and enzyme codes. The top BLASTx hits were used to guide protein tranlations of 39,765 genes and, for the 12,246 contigs lacking significant similarity, the longest ORFs among six strands were translated. For BLASTp searches of NR, contigs were translated based on BLASTx results or, in the case of little or no significant sequence homology, the longest ORFs were used. Transeq 5.0.0 was used to translate ORFs within all contigs in all frames for the mass spectrometry database (below) (51)(52). Gene Ontology annotations were via blast2Go.

Protein extraction and mass spectrometry identification. Total soluble protein was extracted from approximately 5 g Wiley ground wood samples using the NoviPure Soil Protein Extraction kit (MO BIO, Qiagen Carlsbad, CA, catalogue # 30000-20). NanoLC-MS/MS was used to identify proteins in as described (53-55).

Crude protein extracts were further purified with TCA precipitation followed by multiple acetone washes. The pellets were resolubilized to [~1mg/ml] of dry weight:liquid with 8M Urea and aliquots taken for protein concentration determination (PIERCE™ 660nm Protein Assay kit, ThermoFisher Scientific). 25µg of urea solubilized protein extract was 10x concentrated with liquid/liquid extraction (methanol:chloroform:water), trypsin/LysC digested, OMIX C18 SPE cleaned up (Agilent Technologies) and finally 1.5µg loaded for nanoLC-MS/MS analysis using an Agilent 1100 nanoflow

system (Agilent Technologies) connected to a hybrid linear ion trap-orbitrap mass spectrometer (LTQ-Orbitrap Elite™, ThermoFisher Scientific) equipped with an EASY-Spray™ electrospray source. Chromatography of peptides prior to mass spectral analysis was accomplished using capillary emitter column (PepMap® C18, 3µM, 100Å, 150x0.075mm, Thermo Fisher Scientific) onto which 2µl of purified peptides was automatically loaded. NanoHPLC system delivered solvents A: 0.1% (v/v) formic acid , and B: 99.9% (v/v) acetonitrile, 0.1% (v/v) formic acid at 0.50 µL/min to load the peptides (over a 30 minute period) and 0.3µl/min to elute peptides directly into the nano-electrospray with gradual gradient from 3% (v/v) B to 20% (v/v) B over 154 minutes and concluded with 12 minute fast gradient from 20% (v/v) B to 50% (v/v) B at which time a 5 minute flash-out from 50-95% (v/v) B took place. As peptides eluted from the HPLC-column/electrospray source survey MS scans were acquired in the Orbitrap with a resolution of 120,000 followed by MS/MS fragmentation of 20 most intense peptides detected in the precursor MS1 scan from 380 to 1800 m/z; redundancy was limited by dynamic exclusion. Raw data files were imported into Thermo Proteome Discoverer (PD version 2.2.0.388) for database searching and assignment of identification significance. A user-defined metagenomic database was compiled from 6 frame translations of 52,011 assembled contigs (>750bp) generating 312,066 protein entries. Sequest HT search engine (within PD) assigned peptide and protein identifications within 1% False Discovery Rate using 15 ppm mass tolerance for peptide and 0.6 Da for a fragment ion mass. Variable methionine oxidation with asparagine and glutamine deamidation plus fixed cysteine carbamidomethylation was specified. Further stringency for an acceptable identification was applied by requiring at least two peptides per individual protein and Xcorr value of 1.8 or greater per individual peptide spectrum match. The raw mass spectrometry data was deposited to Chorus repository (chorusproject.org, ID#1478) for public sharing and visualization.

343 It should be noted that under the conditions employed, mass spectrometry detection of extracellular
344 proteins is subject to false negative results due to the frequency of trypsin cleavage, low molecular
345 weight, substrate binding and/or proteolytic degradation. False positive results in contrast, are unlikely.
346 The potential activity of 10 extracellular wood-degrading enzymes was quantified on a limited
347 amount of ground sample (<40 mg dry weight) from each location: cellobiohydrolase (CBH, an
348 exocellulase), β-glucosidase (BG, which hydrolyzes cellobiose into glucose), α-glucosidase (AG,
349 which hydrolyzes starch), β-xylosidase (BX, which degrades the xylose component of hemicellulose),
350 β-glucuronidase (BGLU, which degrades the beta-glucuronic acid component of hemicellulose), β-N-
351 acetyl-glucosaminidase (NAG, which breaks down chitin), acid phosphatase (AP, which releases
352 inorganic phosphate from organic matter), leucine-aminopeptidase (LAP, which breaks down
353 polypeptides), polyphenol oxidase (PPO, which oxidizes phenols), and peroxidase (PER, including
354 oxidases that degrade lignin). Samples were stored frozen at −80°C after collection and analyzed as
355 described (56), with the following modification: to ensure detectable activity, the LAP assay was
356 conducted in 0.2M phosphate buffer, pH 6.8, with 1 mM fluorogenic substrate. All enzyme activities
357 were calculated as nmol activity per g per hr and ln-transformed prior to interpretation.
358
359
360
361 **ACKNOWLEDGMENTS**
362 The work conducted by the U.S. Department of Energy Joint Genome Institute, a DOE Office of
363 Science User Facility, is supported by the Office of Science of the U.S. Department of Energy under
364 Contract No. DE-AC02-05CH11231. Research was also supported by NSF grants 1457695 and
365 1457721 to JMB and DC, respectively, and by JSPS Grants-in-Aid for Scientific Research 16K18727

366 to CH. The research in Martin Lab was funded by the French National Research Agency through the
367 project SYMWOOD (Laboratory of Excellence Advanced Research on the Biology of Tree and Forest
368 Ecosystems, ANR-11-LABX 0002 01).
369
370 We thank Forest Service staff Robin Taylor-Davenport for identifying ground cover vegetation and
371 Helen Smith for collecting samples at Tenderfoot Creek Experimental Forest.

Table 1. Metatranscriptome and Metaproteome summary

RNA-seq reads	291,596,160
Contigs > 100 reads	274,233
Average length, bp	590
Contigs >100 reads; >750bp	52,011
IPR domains	42,307
GO assignments	33,523
GO after merging	116,997
Confirmed IPS GOs	103,837
EC assignments	7,901
Oxidoreductases	2,083
Transferases	1,553
Hydrolases	3,242
Lyases	556
Isomerases	389
Ligases	281
TMHs predicted	10,510
Eukaryotic secretion signal	2,705
Protein detected[1]	1,935

[1]Mass spectroscopy detected proteins using 6-frame translated contigs.

Table 2. Contigs predicted to encode proteins with Auxiliary Activities (AA) ordered by sequences reads.[1]

Contig	Reads	Length	Family [2]	Putative function	e-Value[3]	Sim mean, %[4]	Comment[5]
5367253_3	10056	1225	AA3_3	Methanol oxidase	0	93.1	MS
2929739_1	9675	873	AA9	LPMO	3.35E-54	57.9	SS
1507360_1	9562	1007	AA6	Benzoquinone reductase	5.87E-86	75.1	MS
4793784_4	8517	892	AA2	Manganese peroxidase	7.12E-98	73.5	
3105967_1	8470	824	AA9	LPMO	6.42E-95	70.8	SS
1303515_1	7776	1316	AA2	Manganese peroxidase	1.91E-158	76	
798557_1	7736	1563	AA3_3	Alcohol oxidase	0	90.8	MS
4253668_1	7400	862	AA9	LPMO	4.27E-113	76.1	SS
1203164_1	6279	820	AA9	LPMO	1.78E-72	84.1	CBM1
694467_2	5891	1568	AA9	LPMO	5.19E-68	72.2	
3968694_1	5536	1140	AA2	Manganese peroxidase	2.44E-114	77.9	
3834150_1	5521	862	AA6	Benzoquinone reductase	5.01E-103	82.9	MS
3968694_2	5211	1057	AA2	Manganese peroxidase	1.94E-80	76.4	
3406352_1	4719	1151	AA2	Manganese peroxidase	1.00E-128	75	
536886_1	4574	1455	AA3_3	Alcohol oxidase	0	93.8	MS
5221162_1	4332	865	AA9	LPMO	4.28E-36	65.7	
4793784_3	4023	932	AA2	Manganese peroxidase	7.40E-106	72.2	MS
1201987_1	3747	1074	AA9	LPMO	5.11E-116	83.2	SS
2929739_3	3640	915	AA9	LPMO	1.91E-47	60.4	SS; MS
2280897_3	3374	1119	AA3_3	Alcohol oxidase	0	92.8	MS
4793784_1	3310	901	AA2	Manganese peroxidase	3.24E-92	71.3	MS
4582340_1	3263	929	AA9	LPMO	2.36E-83	82	CBM1
2280897_7	3087	1095	AA3_3	Alcohol oxidase	8.37E-148	92	MS
798557_5	3018	1095	AA3_3	Alcohol oxidase	0	87.6	MS
1303515_3	2984	1055	AA2	Manganese peroxidase	1.35E-119	80.1	
2353562_1	2843	1263	AA3	GMC oxidoreductase	3.97E-59	50.4	
3751681_1	2838	912	AA9	LPMO	2.47E-100	79.7	SS
798557_17	2693	1051	AA3_3	Alcohol oxidase	9.20E-171	89	MS
4109481_1	2461	1271	AA3_2	GMC oxidoreductase	1.38E-111	65.3	

1227884_4	2455	1033	AA3_3	Alcohol oxidase	1.06E-175	91	MS

[1]Complete information, including BLASTx analyses, Interpro and Gene Ontology designations, and mass spectrometry results are listed in supplemental Dataset S1.

[2]CAZy families identified by dbCAN (Yin et al 2012 NAR doi: 10.1093/nar/gks479)

[3]e-value of top BLASTx hit.

[4]Average sequence similarity to the top ten BLASTx hits.

[5]SS, SignalP determined secretion signal; MS, LC-MS/MS identified proteins; CBM1, Carbohydrate Binding Module family 1.

386

Table 3. Contigs predicted to encode glycoside hydrolases (GH) ordered by sequences reads[1]

Contig	Reads	Length	Family[2]	Putative function	e-Value[3]	sim mean, %[4]	comment[5]
3240852_1	42911	1551	GH7	Cellobiohydrolase 1	0	78.6	SS; MS
6091156_1	25158	1281	GH6	Cellobiohydrolase 2	2.21E-98	59.3	SS; MS
4924579_1	24747	1587	GH13	1,4-α-glucan branching enzyme	0	88.8	
94066_1	24422	1169	GH5	Endo-β-1,4-glucanase	1.91E-134	69.5	SS
4034495_1	23449	1472	GH45	Endo-β-1,4-glucanase	2.51E-32	56.9	SS
4921502_1	19419	1252	GH5_5	Endo-β -1,4-glucanase	8.65E-160	83	SS; MS
5743057_1	18678	845	GH12	Endo-β 1,4-glucanase	2.54E-115	77.9	SS; MS
4739131_4	17714	1657	GH5	Glycoside hydrolase	2.11E-74	54.9	SS
1384861_1	16216	1295	GH6	Cellobiohydrolase 2	1.57E-88	58.1	SS; MS
6836211_1	15440	1335	GH18	Chitinase	1.49E-62	64.2	
3859657_1	14542	1457	GH114	Endoα-1,4 polygalactosaminidase	8.40E-90	69.5	
3529359_1	14380	1570	GH16	β–1,3-glucanase	1.72E-109	68.5	SS
3589366_1	13195	1464	GH7	Cellobiohydrolase 1	0	78.5	SS; MS
3098980_1	13193	1072	GH16	Endo-1,3- β-glucanase	2.52E-106	70.4	
2908735_1	10927	1113	GH79	Glycoside hydrolase	1.82E-74	68.1	
3561636_2	9572	1222	GH10	Endo-1,4-β xylanase	9.07E-158	69.7	SS
65078_1	9266	1125	GH7	Cellobiohydrolase 1	1.99E-144	75.9	CBM1
5394650_1	8876	1568	GH5_22	Glycoside hydrolase	1.36E-81	66	
1142146_1	8843	1125	GH5_5	Endo-β -1,4-glucanase	1.97E-151	76.8	
4728183_1	8453	1939	GH128	Glycoside hydrolase	1.89E-125	70.9	SS
98832_1	7998	943	GH128	Glycoside hydrolase	5.62E-88	65.9	
2374420_1	7848	1075	GH9	Glycoside hydrolase	3.18E-50	52.2	
2989759_1	7548	1266	GH128	Glycoside hydrolase	1.48E-50	52.2	
247968_1	7473	1442	GH5_40	Glycoside hydrolase	2.96E-70	58.1	CBM8
4884037_2	7291	965	GH53	Endo-1,4- β-galactanase	2.92E-151	76.6	
5204286_1	6982	1044	GH128	Glycoside hydrolase	3.96E-103	66.8	

830359_1	6946	1312	GH1	β-glucosidase	1.70E-140	68.5	
3175817_1	6832	1625	GH5_7	Endo-1,4- β-mannanase	0	80.1	SS; MS
2132535_1	6435	1193	GH105	Glycoside hydrolase	4.62E-107	66.9	
1970615_2	5800	1048	GH7	Cellobiohydrolase 1	1.47E-134	76.5	MS

[1]Complete information, including BLASTx analyses, Interpro and Gene Ontology designations, and mass spectrometry results are listed in supplemental Dataset S1.

[2]CAZy families identified by dbCAN (Yin et al 2012 NAR doi: 10.1093/nar/gks479)

[3]e-value of the top BLASTx hit.

[4]Average sequence similarity to the top ten BLASTx hits.

[5]SS, SignalP determined secretion signal; MS, LC-MS/MS identified proteins; CBM, Carbohydrate Binding Module family.

395

Table 4. Glycoside hydrolases identified in decayed *Pinus contorta* by mass spectrometry[1]

Contig and frame	Reads	Length	CAZy family	e-Value[2]	Coverage [%]	# Pept	# PSMs	Unique Pept	Sequest HT score
4346763_2_5	1289	974	GH1	1.77E-123	12	3	5	3	13
4346763_4_2	134	980	GH1	5.00E-117	12	3	5	3	13
4346763_3_1	708	993	GH1	8.16E-121	9	2	3	2	8
4459897_1_1	260	884	GH10	1.63E-72	15	3	7	3	20
3889902_1_4	3745	1235	GH10	1.18E-172	7	2	5	2	17
2058669_1_6	2552	1145	GH10	8.35E-98	8	2	2	2	7
3960173_1_1	602	936	GH12	2.08E-142	6	2	4	2	12
3166842_1_5	1268	1146	GH17	1.92E-145	14	3	5	3	15
2491547_1_6	1188	1068	GH3	8.07E-91	13	2	5	2	5
3730185_1_5	1252	831	GH47	8.13E-166	8	2	3	2	8
6091156_1_3	25158	1281	GH6	2.70E-100	23	5	24	4	73
1553595_1_2	2108	926	GH6	5.22E-156	11	2	7	2	24
1384861_1_6	16216	1295	GH6	1.13E-102	8	2	4	1	8
1384861_2_1	4220	1303	GH6	2.48E-103	5	2	3	1	7
658106_4_6	1932	1273	GH7	1.72E-137	17	5	24	4	74
658106_7_2	1550	1024	GH7	1.50E-97	16	4	23	3	70
3240852_1_4	42911	1551	GH7	0	20	7	23	6	63
4852_1_6	697	764	GH7	3.56E-70	11	2	12	1	34
3223568_3_6	477	871	GH7	6.16E-115	10	2	9	1	26
3240852_2_6	1163	965	GH7	1.59E-104	16	3	9	3	26

1970615_2_6	5800	1048	GH7	2.18E-142	18	4	5	3	13
3589366_2_3	1295	1109	GH7	4.77E-168	14	3	3	2	5
3589366_1_6	13195	1464	GH7	0	6	2	2	1	4

396 [2]BLASTp NR

397

398

Table 5. Redox enzymes potentially involved in lignocellulose degradation identified in decayed *Pinus contorta* by mass spectrometry.

Contig and frame	Read	Length	Description	CAZy family	e-Value[2]	Coverage [%]	Pept	PSMs	Unique Pept	Sequest HT score
4793784_3_2	4023	932	Manganese peroxidase	AA2	1.68E-159	7	2	3	1	8
4793784_13_2	2332	1097	Manganese peroxidase	AA2	0	8	2	3	1	9
2280897_3_6	3374	1119	Alcohol oxidase	AA3_3	0	26	8	23	8	66
2280897_9_1	1468	1170	Alcohol oxidase	AA3_3	0	20	6	11	5	34
798557_1_1	7736	1563	Alcohol oxidase	AA3_3	0	15	5	10	2	27
798557_5_2	3018	1095	Alcohol oxidase	AA3_3	0	17	4	8	1	20
798557_13_6	1908	1337	Alcohol oxidase	AA3_3	0	11	3	6	1	15
798557_17_6	2693	1051	Alcohol oxidase	AA3_3	2.12E-166	18	3	6	1	16
2280897_7_2	3087	1095	Alcohol oxidase	AA3_3	1.83E-177	11	2	5	1	15
2280897_11_6	1698	1169	Alcohol oxidase	AA3_3	0	9	3	3	2	9
798557_25_4	176	899	Alcohol oxidase	AA3_3	7.64E-157	13	2	5	0	12
536886_1_6	4574	1455	Alcohol oxidase	AA3_3	0	9	3	7	3	22
2766776_1_4	910	784	Benzoquinone reductase	AA6	7.36E-98	12	2	2	2	6
3005685_1_6	258	810	Benzoquinone reductase	AA6	6.80E-87	10	2	12	1	34
1341126_2_3	1595	1039	Benzoquinone reductase	AA6	7.50E-120	26	6	26	5	76
1507360_1_3	9562	1007	Benzoquinone reductase	AA6	1.28E-109	21	5	19	4	56
1507360_2_6	263	993	Benzoquinone reductase	AA6	2.95E-70	12	3	14	2	39
3719648_4_6	986	1106	Benzoquinone reductase	AA6	6.41E-111	27	8	43	7	123
1712785_3_2	1051	816	Benzoquinone reductase	AA6	8.34E-112	28	5	34	4	99
1712785_2_4	739	948	Benzoquinone reductase	AA6	5.49E-144	20	5	24	4	71

3711757_1_4	925	885	NADH-quinone OR	AA6	1.86E-106	7	2	10	1	27
3834150_1_3	5521	862	Benzoquinone reductase	AA6	9.20E-111	8	2	10	2	30
3719648_1_3	1059	828	NADH-quinone OR	AA6	5.06E-82	12	3	11	2	29
4644641_1_2	2872	842	Dyp-type peroxidase		3.56E-93	37	8	37	6	109
4644641_2_5	1109	863	Dyp-type peroxidase		4.33E-79	33	5	32	3	85
3735866_1_2	448	873	Dyp-type peroxidase		6.27E-45	20	3	17	2	51
3427787_2_2	1036	1107	Dyp-type peroxidase		1.96E-81	28	6	9	5	29

399 [2]BLASTp NR

400 **REFERENCES**

401 1. Ottosson E, Norden J, Dahlberg A, Edman M, Jonsson M, Larsson KH, Olsson J, Penttila R, Stenlid
402 J, Ovaskainen O. 2014. Species associations during the succession of wood-inhabiting fungal
403 communities. Fungal Ecology 11:17-28.
404 2. Arnstadt T, Hoppe B, Kahl T, Kellner H, Kruger D, Bauhus J, Hofrichter M. 2016. Dynamics of
405 fungal community composition, decomposition and resulting deadwood properties in logs of
406 *Fgus sylvatica, Picea abies* and *Pinus sylvestris*. Forest Ecology and Management 382:129-142.
407 3. Lindner DL, Vasaitis R, Kubartova A, Allmer J, Johannesson H, Banik MT, Stenlid J. 2011. Initial
408 fungal colonizer affects mass loss and fungal community development in *Picea abies* logs 6 yr
409 after inoculation. Fungal Ecology 4:449-460.
410 4. Rajala T, Tuomivirta T, Pennanen T, Makipaa R. 2015. Habitat models of wood-inhabiting fungi
411 along a decay gradient of Norway spruce logs. Fungal Ecology 18:48-55.
412 5. Rajala T, Peltoniemi M, Hantula J, Makipaa R, Pennanen T. 2011. RNA reveals a succession of
413 active fungi during decay of Norway spruce logs. Fungal Ecology 4:437-448.
414 6. Vetrovsky T, Stursova M, Baldrian P. 2016. Fungal communities in soils: Soil organic matter
415 degradation. Methods Mol Biol 1399:89-100.
416 7. Damon C, Lehembre F, Oger-Desfeux C, Luis P, Ranger J, Fraissinet-Tachet L, Marmeisse R. 2012.
417 Metatranscriptomics reveals the diversity of genes expressed by eukaryotes in forest soils. PLoS
418 One 7:e28967.
419 8. Zifcakova L, Vetrovsky T, Howe A, Baldrian P. 2016. Microbial activity in forest soil reflects the
420 changes in ecosystem properties between summer and winter. Environ Microbiol 18:288-301.

9. Hesse CN, Mueller RC, Vuyisich M, Gallegos-Graves LV, Gleasner CD, Zak DR, Kuske CR. 2015. Forest floor community metatranscriptomes identify fungal and bacterial responses to N deposition in two maple forests. Front Microbiol 6:10.3389/fmicb.2015.00337.

10. Keiblinger KM, Fuchs S, Zechmeister-Boltenstern S, Riedel K. 2016. Soil and leaf litter metaproteomics-a brief guideline from sampling to understanding. FEMS Microbiol Ecol 92:10.1093/femsec/fiw180.

11. Bastida F, Torres IF, Moreno JL, Baldrian P, Ondono S, Ruiz-Navarro A, Hernandez T, Richnow HH, Starke R, Garcia C, Jehmlich N. 2016. The active microbial diversity drives ecosystem multifunctionality and is physiologically related to carbon availability in Mediterranean semi-arid soils. Mol Ecol 25:4660-73.

12. Cullen D. 2014. Wood decay, p 41-62. *In* Martin F (ed), Ecological genomics of fungi. Wiley-Blackwell, New York.

13. Hatakka A, Hammel KE. 2010. Fungal biodegradation of lignocelluloses. *In* Hofrichter M (ed), Industrial Applications, 2 ed, vol 10. Springer-Verlag, Berlin.

14. Lombard V, Golaconda Ramulu H, Drula E, Coutinho PM, Henrissat B. 2014. The carbohydrate-active enzymes database (CAZy) in 2013. Nucleic Acids Res 42:D490-D495.

15. Riley R, Salamov AA, Brown DW, Nagy LG, Floudas D, Held BW, Levasseur A, Lombard V, Morin E, Otillar R, Lindquist EA, Sun H, LaButti KM, Schmutz J, Jabbour D, Luo H, Baker SE, Pisabarro AG, Walton JD, Blanchette RA, Henrissat B, Martin F, Cullen D, Hibbett DS, Grigoriev IV. 2014. Extensive sampling of basidiomycete genomes demonstrates inadequacy of the white-rot/brown-rot paradigm for wood decay fungi. Proc Natl Acad Sci U S A 111:9923-8.

16. Floudas D, Binder M, Riley R, Barry K, Blanchette RA, Henrissat B, Martinez AT, Otillar R, Spatafora JW, Yadav JS, Aerts A, Benoit I, Boyd A, Carlson A, Copeland A, Coutinho PM, de Vries RP, Ferreira P, Findley K, Foster B, Gaskell J, Glotzer D, Gorecki P, Heitman J, Hesse C, Hori C, Igarashi K, Jurgens JA, Kallen N, Kersten P, Kohler A, Kues U, Kumar TK, Kuo A, LaButti K, Larrondo LF, Lindquist E, Ling A, Lombard V, Lucas S, Lundell T, Martin R, McLaughlin DJ, Morgenstern I, Morin E, Murat C, Nagy LG, Nolan M, Ohm RA, Patyshakuliyeva A, et al. 2012. The Paleozoic origin of enzymatic lignin decomposition reconstructed from 31 fungal genomes. Science 336:1715-9.

17. Plett JM, Kemppainen M, Kale SD, Kohler A, Legue V, Brun A, Tyler BM, Pardo AG, Martin F. 2011. A secreted effector protein of *Laccaria bicolor* is required for symbiosis development. Curr Biol 21:1197-203.

18. Levasseur A, Drula E, Lombard V, Coutinho PM, Henrissat B. 2013. Expansion of the enzymatic repertoire of the CAZy database to integrate auxiliary redox enzymes. Biotechnol Biofuels 6:41.

19. Daniel G, Volc J, Filonova L, Plihal O, Kubatova E, Halada P. 2007. Characteristics of *Gloeophyllum trabeum* alcohol oxidase, an extracellular source of H2O2 in brown rot decay of wood. Appl Environ Microbiol 73:6241-53.

20. Shimokawa T, Nakamura M, Hayashi N, Ishihara M. 2004. Production of 2,5-dimethoxyhydroquinone by the brown-rot fungus *Serpula lacrymans* to drive extracellular Fenton reaction. Holzforschung 58:305-310.

21. Suzuki MR, Hunt CG, Houtman CJ, Dalebroux ZD, Hammel KE. 2006. Fungal hydroquinones contribute to brown rot of wood. Environ Microbiol 8:2214-23.

22. Varela E, Tien M. 2003. Effect of pH and oxalate on hydroquinone-derived hydroxyl radical formation during brown rot wood degradation. Appl Environ Microbiol 69:6025-31.

23. Meier KK, Jones SM, Kaper T, Hansson H, Koetsier MJ, Karkehabadi S, Solomon EI, Sandgren M, Kelemen B. 2018. Oxygen activation by Cu LPMOs in recalcitrant carbohydrate polysaccharide conversion to monomer sugars. Chem Rev 118:2593-2635.

24. Linde D, Ruiz-Duenas FJ, Fernandez-Fueyo E, Guallar V, Hammel KE, Pogni R, Martinez AT. 2015. Basidiomycete DyPs: Genomic diversity, structural-functional aspects, reaction mechanism and environmental significance. Arch Biochem Biophys 574:66-74.

25. Schneider T, Keiblinger KM, Schmid E, Sterflinger-Gleixner K, Ellersdorfer G, Roschitzki B, Richter A, Eberl L, Zechmeister-Boltenstern S, Riedel K. 2012. Who is who in litter decomposition? Metaproteomics reveals major microbial players and their biogeochemical functions. ISME J 6:1749-62.

26. Kubartova A, Ottosson E, Stenlid J. 2015. Linking fungal communities to wood density loss after 12 years of log decay. FEMS Microbiol Ecol 91.

27. Lindner D, Vasaitis R, Kubartova A, Allmer J, Johannesson H, Banik M, Stenlid J. 2011. Initial fungal colonizer affects mass loss and fungal community development in *Picea abies* logs after 6 years. Fungal Ecology 4:449-460.

28. Makipaa R, Rajala T, Schigel D, Rinne KT, Pennanen T, Abrego N, Ovaskainen O. 2017. Interactions between soil- and dead wood-inhabiting fungal communities during the decay of Norway spruce logs. ISME J 11:1964-1974.

29. Liao HL, Chen Y, Bruns TD, Peay KG, Taylor JW, Branco S, Talbot JM, Vilgalys R. 2014. Metatranscriptomic analysis of ectomycorrhizal roots reveal genes associated with *Piloderma*-

Pinus symbiosis: Improved methodologies for assessing gene expression in situ. Environ Microbiol doi:10.1111/1462-2920.12619.

30. Robicheau BM, Young AP, LaButti K, Grigoriev IV, Walker AK. 2017. The complete mitochondrial genome of the conifer needle endophyte, *Phialocephala scopiformis* DAOMC 229536 confirms evolutionary division within the fungal *Phialocephala fortinii* s.l. - *Acephala appalanata* species complex. Fungal Biol 121:212-221.

31. Schlegel M, Munsterkotter M, Guldener U, Bruggmann R, Duo A, Hainaut M, Henrissat B, Sieber CM, Hoffmeister D, Grunig CR. 2016. Globally distributed root endophyte *Phialocephala subalpina* links pathogenic and saprophytic lifestyles. BMC Genomics 17:1015.

32. Walker AK, Frasz SL, Seifert KA, Miller JD, Mondo SJ, LaButti K, Lipzen A, Dockter RB, Kennedy MC, Grigoriev IV, Spatafora JW. 2016. Full genome of *Phialocephala scopiformis* DAOMC 229536, a fungal endophyte of spruce producing the potent anti-insectan compound rugulosin. Genome Announc 4.

33. Martinez AT. 2002. Molecular biology and structure-function of lignin-degrading heme peroxidases. Enzyme Microb Technol 30:425-444.

34. Janusz G, Pawlik A, Sulej J, Swiderska-Burek U, Jarosz-Wilkolazka A, Paszczynski A. 2017. Lignin degradation: microorganisms, enzymes involved, genomes analysis and evolution. FEMS Microbiol Rev 41:941-962.

35. Hofrichter M, Ullrich R, Pecyna MJ, Liers C, Lundell T. 2010. New and classic families of secreted fungal heme peroxidases. Appl Microbiol Biotechnol 87:871-97.

505 36. Kellner H, Luis P, Pecyna MJ, Barbi F, Kapturska D, Kruger D, Zak DR, Marmeisse R, Vandenbol M,
506 Hofrichter M. 2014. Widespread occurrence of expressed fungal secretory peroxidases in forest
507 soils. PLoS One 9:e95557.
508 37. Kojima Y, Varnai A, Ishida T, Sunagawa N, Petrovic DM, Igarashi K, Jellison J, Goodell B, Alfredsen
509 G, Westereng B, Eijsink VG, Yoshida M. 2016. A lytic polysaccharide monooxygenase with broad
510 xyloglucan specificity from the brown-rot fungus *Gloeophyllum trabeum* and its action on
511 cellulose-xyloglucan complexes. Appl Environ Microbiol 82:6557-6572.
512 38. Bissaro B, Rohr AK, Muller G, Chylenski P, Skaugen M, Forsberg Z, Horn SJ, Vaaje-Kolstad G,
513 Eijsink VGH. 2017. Oxidative cleavage of polysaccharides by monocopper enzymes depends on
514 H2O2. Nat Chem Biol 13:1123-1128.
515 39. Presley GN, Zhang J, Schilling JS. 2016. A genomics-informed study of oxalate and cellulase
516 regulation by brown rot wood-degrading fungi. Fungal Genet Biol doi:10.1016/j.fgb.2016.08.004.
517 40. Kaneko S, Yoshitake K, Itakura S, Tanaka H, Enoki A. 2005. Relationship between production of
518 hydroxyl radicals and degradation of wood, crystalline cellulose, and lignin-related compound or
519 accumulation of oxalic acid in cultures of brown-rot fungi. J Wood Sci 51:262-269.
520 41. Jensen KA, Jr., Houtman CJ, Ryan ZC, Hammel KE. 2001. Pathways for extracellular Fenton
521 chemistry in the brown rot basidiomycete *Gloeophyllum trabeum*. Appl Environ Microbiol
522 67:2705-11.
523 42. Wei D, Houtman CJ, Kapich AN, Hunt CG, Cullen D, Hammel KE. 2009. Laccase and its role in
524 production of extracellular reactive oxygen species during wood decay by the brown rot
525 basidiomycete *Postia placenta*. Appl Environ Microbiol 76:2091-7.

526 43. Vaaje-Kolstad G, Westereng B, Horn SJ, Liu Z, Zhai H, Sorlie M, Eijsink VG. 2010. An oxidative
527 enzyme boosting the enzymatic conversion of recalcitrant polysaccharides. Science 330:219-22.
528 44. Song B, Li B, Wang X, Shen W, Park S, Collings C, Feng A, Smith SJ, Walton JD, Ding SY. 2018. Real-
529 time imaging reveals that lytic polysaccharide monooxygenase promotes cellulase activity by
530 increasing cellulose accessibility. Biotechnol Biofuels 11:41.
531 45. Kubartova A, Ottosson E, Dahlberg A, Stenlid J. 2012. Patterns of fungal communities among and
532 within decaying logs, revealed by 454 sequencing. Mol Ecol 21:4514-32.
533 46. Rajala T, Peltoniemi M, Pennanen T, Makipaa R. 2012. Fungal community dynamics in relation to
534 substrate quality of decaying Norway spruce (*Picea abies* [L.] Karst.) logs in boreal forests. FEMS
535 Microbiol Ecol 81:494-505.
536 47. Hoppe B, Krger K, Kahl T, Arnstadt T, Buscot F, Bauhus J, Wubet T. 2015. A pyrosequencing insight
537 into sprawling bacterial diversity and community dynamics in decaying deadwood logs of *Fagus*
538 *sylvatica* and *Picea abies*. Sci Rep 5:9456.
539 48. Valaskova V, de Boer W, Gunnewiek PJ, Pospisek M, Baldrian P. 2009. Phylogenetic composition
540 and properties of bacteria coexisting with the fungus *Hypholoma fasciculare* in decaying wood.
541 ISME J 3:1218-21.
542 49. Johnston SR, Boddy L, Weightman AJ. 2016. Bacteria in decomposing wood and their interactions
543 with wood-decay fungi. Fems Microbiology Ecology 92.
544 50. Lieu PJ, Kelsey RG, Shafizadeh F. 1979. Some chemical characteristics of green and dead
545 lodgepole pine and western white pine. Service UF, Intermountain Forest and Range Experiment
546 Station, Ogden, Utah.

51. Rice P, Longden I, Bleasby A. 2000. EMBOSS: the European Molecular Biology Open Software Suite. Trends Genet 16:276-7.

52. Blankenberg D, Taylor J, Schenck I, He J, Zhang Y, Ghent M, Veeraraghavan N, Albert I, Miller W, Makova KD, Hardison RC, Nekrutenko A. 2007. A framework for collaborative analysis of ENCODE data: making large-scale analyses biologist-friendly. Genome Res 17:960-4.

53. Hori C, Ishida T, Igarashi K, Samejima M, Suzuki H, Master E, Ferreira P, Ruiz-Duenas FJ, Held B, Canessa P, Larrondo LF, Schmoll M, Druzhinina IS, Kubicek CP, Gaskell JA, Kersten P, St John F, Glasner J, Sabat G, Splinter BonDurant S, Syed K, Yadav J, Mgbeahuruike AC, Kovalchuk A, Asiegbu FO, Lackner G, Hoffmeister D, Rencoret J, Gutierrez A, Sun H, Lindquist E, Barry K, Riley R, Grigoriev IV, Henrissat B, Kues U, Berka RM, Martinez AT, Covert SF, Blanchette RA, Cullen D. 2014. Analysis of the *Phlebiopsis gigantea* genome, transcriptome and secretome provides insight into its pioneer colonization strategies of wood. PLoS Genet 10:e1004759.

54. Fernandez-Fueyo E, Ruiz-Duenas FJ, Ferreira P, Floudas D, Hibbett DS, Canessa P, Larrondo LF, James TY, Seelenfreund D, Lobos S, Polanco R, Tello M, Honda Y, Watanabe T, Ryu JS, Kubicek CP, Schmoll M, Gaskell J, Hammel KE, St John FJ, Vanden Wymelenberg A, Sabat G, Splinter BonDurant S, Syed K, Yadav JS, Doddapaneni H, Subramanian V, Lavin JL, Oguiza JA, Perez G, Pisabarro AG, Ramirez L, Santoyo F, Master E, Coutinho PM, Henrissat B, Lombard V, Magnuson JK, Kues U, Hori C, Igarashi K, Samejima M, Held BW, Barry KW, LaButti KM, Lapidus A, Lindquist EA, Lucas SM, Riley R, Salamov AA, et al. 2012. Comparative genomics of *Ceriporiopsis subvermispora* and *Phanerochaete chrysosporium* provide insight into selective ligninolysis. Proc Natl Acad Sci U S A 109:5458-63.

55. Ryu JS, Shary S, Houtman CJ, Panisko EA, Korripally P, St John FJ, Crooks C, Siika-Aho M, Magnuson JK, Hammel KE. 2011. Proteomic and functional analysis of the cellulase system expressed by *Postia placenta* during brown rot of solid wood. Appl Environ Microbiol 77:7933-41.

56. Talbot JM, Martin VJ, Kohler A, Henrissat B, Peay KG. 2015. Functional guild classification predicts the enzymatic role of fungi in litter and soil biogeochemistry. Soil Biology and Biochemistry 88:441-456.

FIGURE LEGENDs

Figure 1. Distribution of 52,011 contigs. Hypotheticals includes conserved hypothetical, predicted proteins and uncharacterized proteins. Transporters include permeases and those assigned to the major facilitator superfamily (MFS)

Figure2. Number of contigs and reads assigned to AA families.

Figure 3. Number of contigs and reads assigned to glycoside hydrolase families known to include cellulases.

Figure 4. Number of contigs and reads assigned to glycoside hydrolase families known to include hemicellulases

590 Figure 5. Distributions of top 30 BLASTp (NR database) hits among translations of all 52,011 contigs
591 (left panel) and for 1,316 contigs (right panel) identified as CAzyme-encoding. The thirty species account
592 for 43% and 54% of the total top hits for all proteins and the CAzyme subset, respectively. White and
593 brown arrows indicate decay type, where known. Fill colors correspond to Basidiomycota (blue),
594 Ascomycota (red) and various other eukaryotes or bacteria (green)
595
596

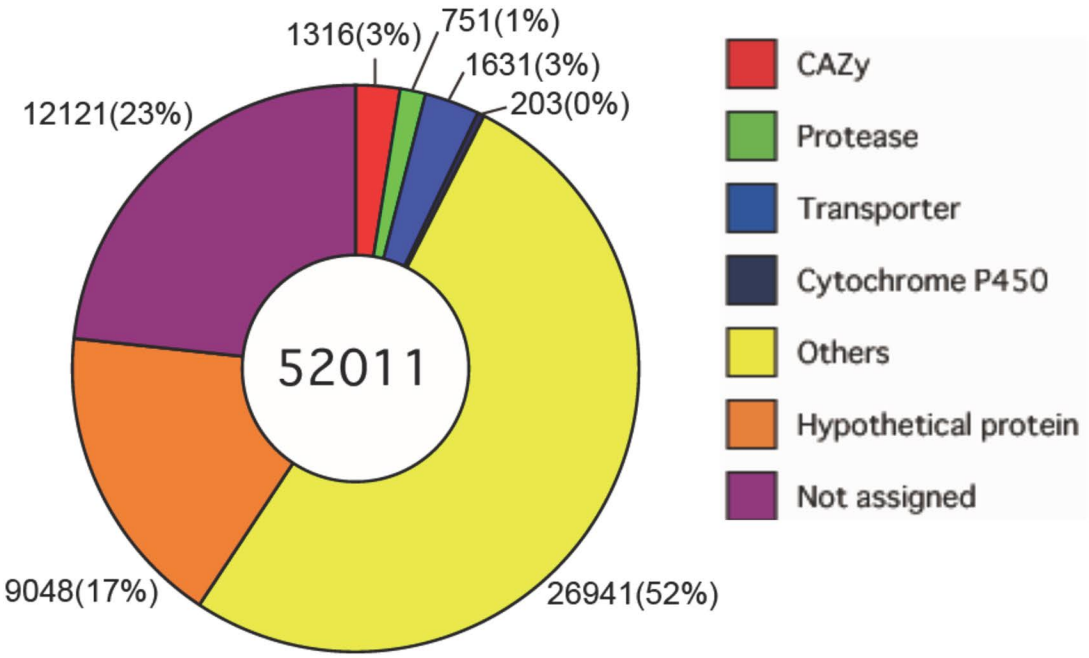
1316(3%)
751(1%)
1631(3%)
203(0%)
12121(23%)
52011
9048(17%)
26941(52%)
CAZy
Protease
Transporter
Cytochrome P450
Others
Hypothetical protein
Not assigned

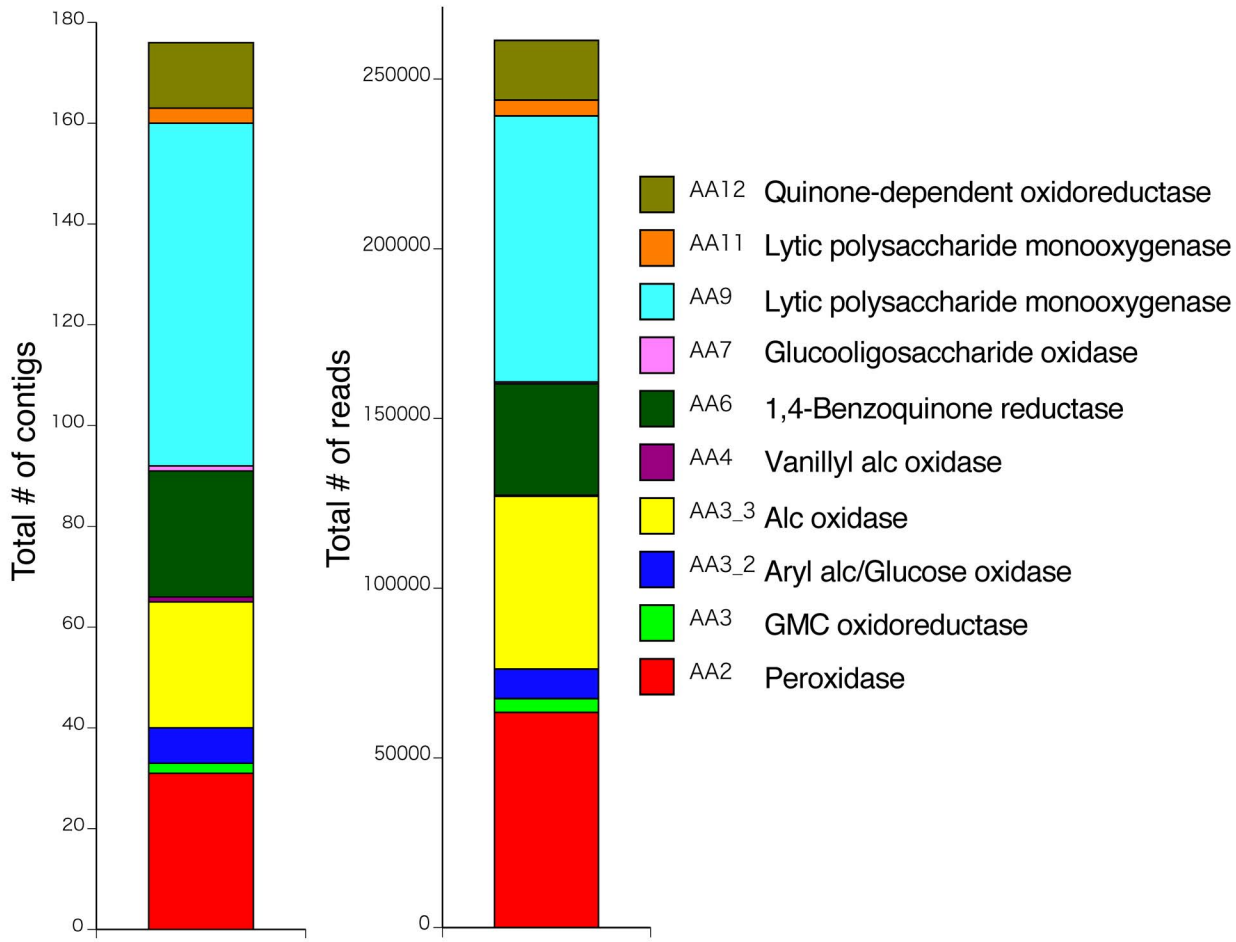
Total # of contigs
180
160
140
120
100
80
60
40
20
0
Total # of reads
250000
200000
150000
100000
50000
0
AA12 Quinone-dependent oxidoreductase
AA11 Lytic polysaccharide monooxygenase
AA9 Lytic polysaccharide monooxygenase
AA7 Glucooligosaccharide oxidase
AA6 1,4-Benzoquinone reductase
AA4 Vanillyl alc oxidase
AA3_3 Alc oxidase
AA3_2 Aryl alc/Glucose oxidase
AA3 GMC oxidoreductase
AA2 Peroxidase

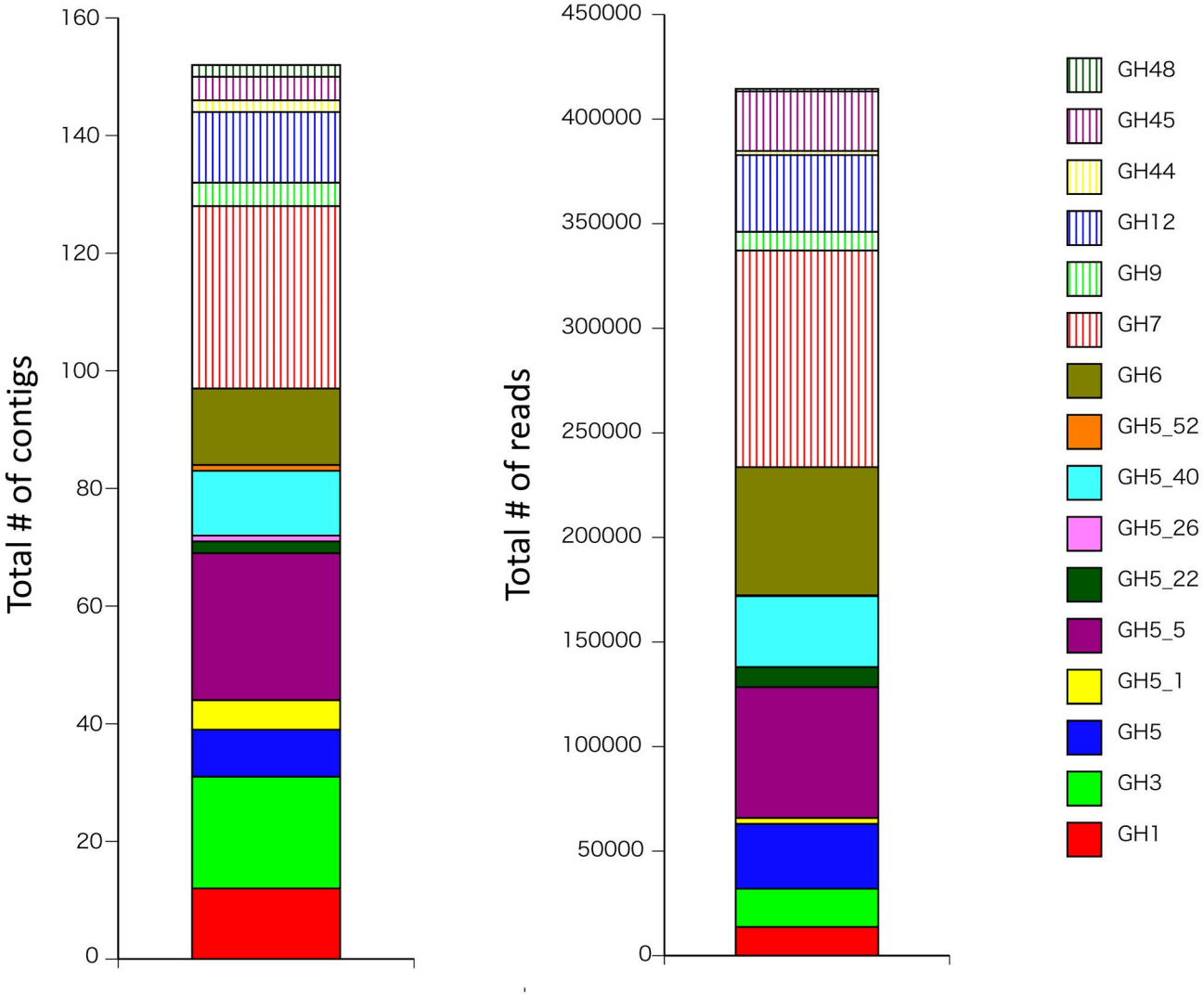
Total # of contigs
160
140
120
100
80
60
40
20
0
Total # of reads
450000
400000
350000
300000
250000
200000
150000
100000
50000
0
GH48
GH45
GH44
GH12
GH9
GH7
GH6
GH5_52
GH5_40
GH5_26
GH5_22
GH5_5
GH5_1
GH5
GH3
GH1

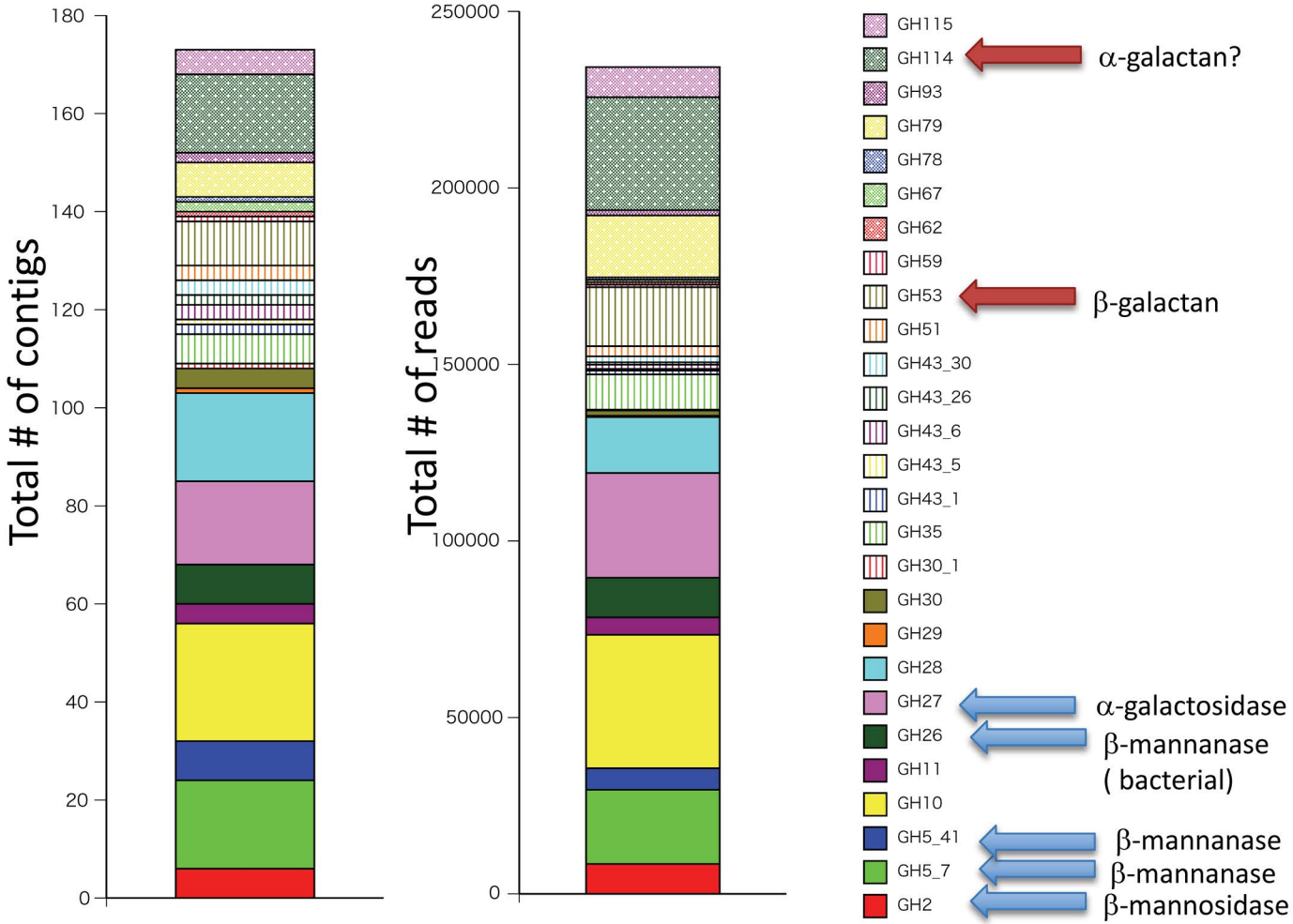
Total # of contigs
180
160
140
120
100
80
60
40
20
0
Total # of reads
250000
200000
150000
100000
50000
0
GH115
GH114
GH93
GH79
GH78
GH67
GH62
GH59
GH53
GH51
GH43_30
GH43_26
GH43_6
GH43_5
GH43_1
GH35
GH30_1
GH30
GH29
GH28
GH27
GH26
GH11
GH10
GH5_41
GH5_7
GH2
α-galactan?
β-galactan
α-galactosidase
β-mannanase
(bacterial)
β-mannanase
β-mannanase
β-mannosidase

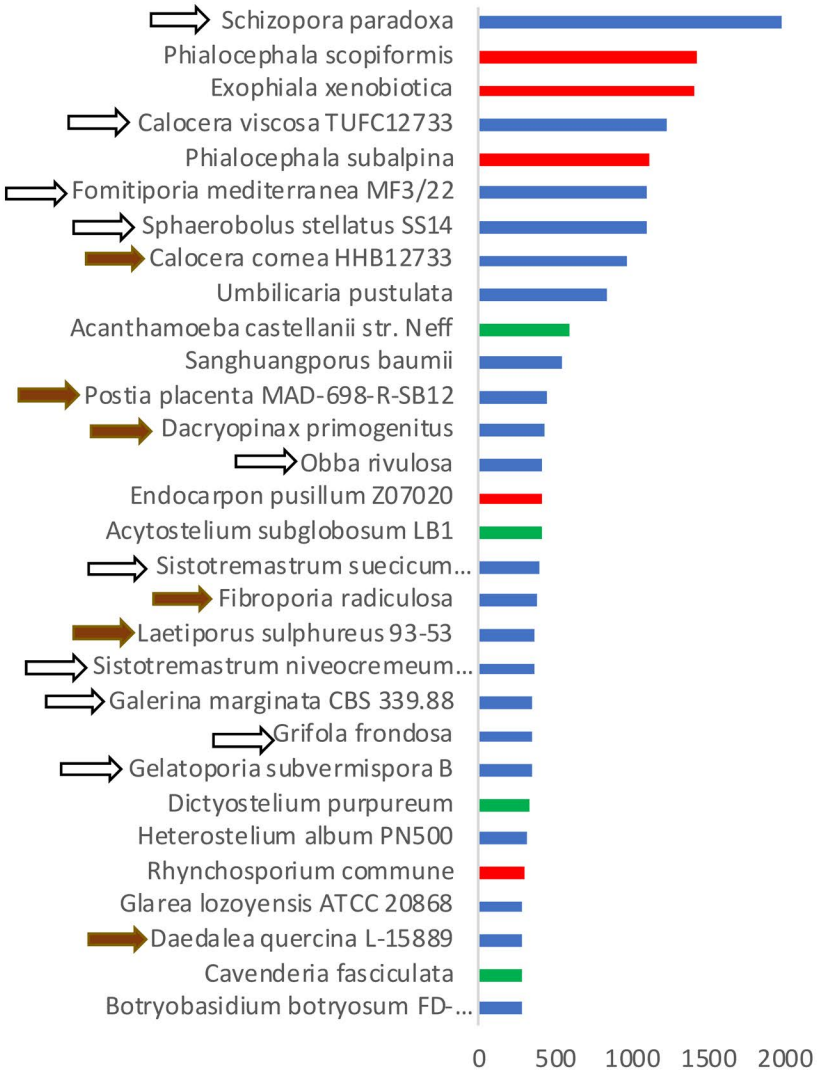
Schizopora paradoxa
Phialocephala scopiformis
Exophiala xenobiotica
Calocera viscosa TUFC12733
Phialocephala subalpina
Fomitiporia mediterranea MF3/22
Sphaerobolus stellatus SS14
Calocera cornea HHB12733
Umbilicaria pustulata
Acanthamoeba castellanii str. Neff
Sanghuangporus baumii
Postia placenta MAD-698-R-SB12
Dacryopinax primogenitus
Obba rivulosa
Endocarpon pusillum Z07020
Acytostelium subglobosum LB1
Sistotremastrum suecicum...
Fibroporia radiculosa
Laetiporus sulphureus 93-53
Sistotremastrum niveocremeum...
Galerina marginata CBS 339.88
Grifola frondosa
Gelatoporia subvermispora B
Dictyostelium purpureum
Heterostelium album PN500
Rhynchosporium commune
Glarea lozoyensis ATCC 20868
Daedalea quercina L-15889
Cavenderia fasciculata
Botryobasidium botryosum FD-...
0
500
1000
1500
2000

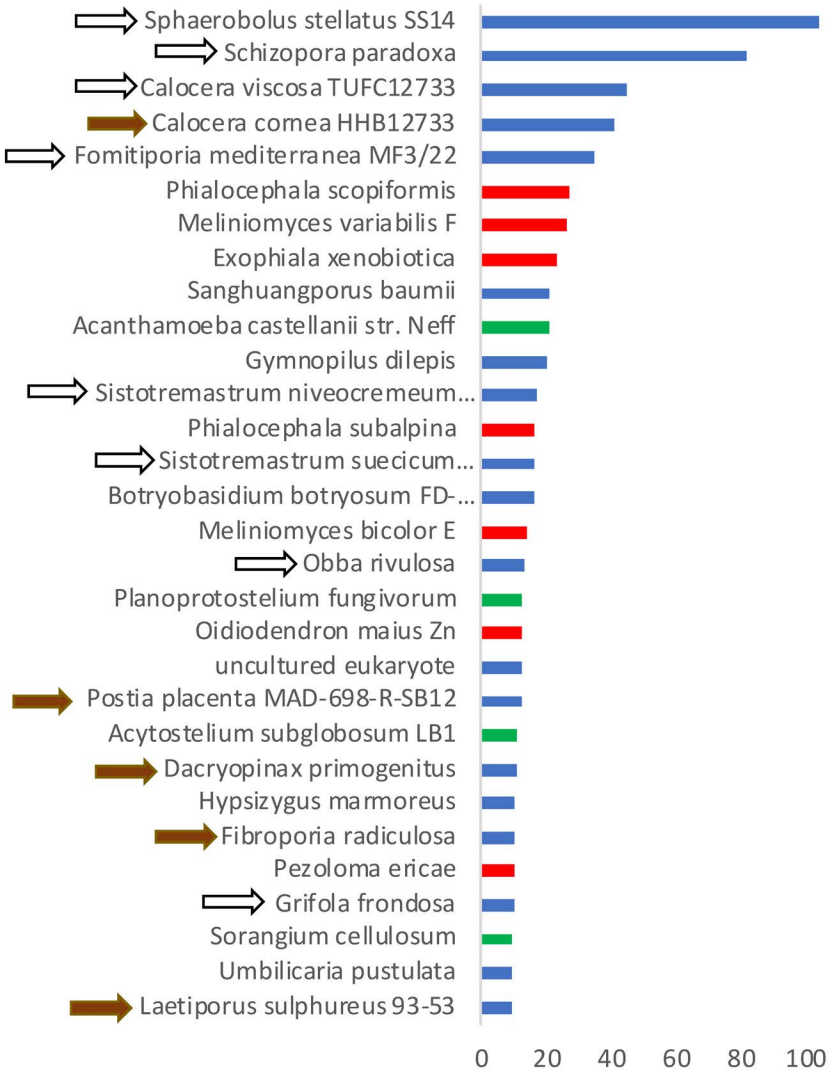
Sphaerobolus stellatus SS14
Schizopora paradoxa
Calocera viscosa TUFC12733
Calocera cornea HHB12733
Fomitiporia mediterranea MF3/22
Phialocephala scopiformis
Meliniomyces variabilis F
Exophiala xenobiotica
Sanghuangporus baumii
Acanthamoeba castellanii str. Neff
Gymnopilus dilepis
Sistotremastrum niveocremeum...
Phialocephala subalpina
Sistotremastrum suecicum...
Botryobasidium botryosum FD-...
Meliniomyces bicolor E
Obba rivulosa
Planoprotostelium fungivorum
Oidiodendron maius Zn
uncultured eukaryote
Postia placenta MAD-698-R-SB12
Acytostelium subglobosum LB1
Dacryopinax primogenitus
Hypsizygus marmoreus
Fibroporia radiculosa
Pezoloma ericae
Grifola frondosa
Sorangium cellulosum
Umbilicaria pustulata
Laetiporus sulphureus 93-53
0
20
40
60
80
100